Available online at www.sciencedirect.com
SCIENCE DIRECT®
Electrochimica Acta 49 (2004) 1105–1112
ELECTROCHIMICA Acta
www.elsevier.com/locate/electacta

Small-angle neutron scattering and cyclic voltammetry study on electrochemically oxidized and reduced pyrolytic carbon

A. Braun [a,b,*], J. Kohlbrecher [c], M. Bärtsch [a], B. Schnyder [a], R. Kötz [a,1], O. Haas [a], A. Wokaun [a,b]

[a] *Electrochemistry Section, General Energy Research Department, Paul Scherrer Institute, CH-5232 Villigen PSI, Switzerland*
[b] *Department of Chemical Engineering and Industrial Chemistry, Swiss Federal Institute of Technology, ETH Zentrum, CH-8092 Zürich, Switzerland*
[c] *ASQ, Spallation Source Division, Paul Scherrer Institute, CH-5232 Villigen PSI, Switzerland*

Received 25 April 2003; received in revised form 23 September 2003; accepted 26 October 2003

Abstract

The electrochemical double layer capacitance and internal surface area of a pyrolytic carbon material after electrochemical oxidation and subsequent reduction was studied with cyclic voltammetry and small-angle neutron scattering. Oxidation yields an enhanced internal surface area (activation), and subsequent reduction causes a decrease of this internal surface area. The change of the Porod constant, as obtained from small-angle neutron scattering, reveals that the decrease in internal surface area is not caused merely by a closing or narrowing of the pores, but by a partial collapse of the pore network.

Keywords: Graphite; Activated carbon; Double layer; Supercapacitors; Small-angle scattering

1. Introduction

Based on the pioneering work by Miklos et al. [1], we have recently published several studies on the oxidation of glassy carbon (GC) for supercapacitor applications [2–14]. GC is a hard carbon material obtained by pyrolysis of phenolic resins and frequently referred to as *pyrolytic* carbon or *vitreous* carbon. Subsequent annealing at high temperatures, which may range from 800 to 3000 °C, has significant influence on the structure of the material [15]. It contains voids of about 1–2 nm dia meter, which are closed and separated against each other [15–17]. The voids (pores) can be opened (*activation*), for instance, by thermochemical gas phase oxidation [1,6–8] or by electrochemical oxidation [2,3]. Oxidation, in this context, means the creation of an open porosity with a very large internal surface, which is often referred to as *activation*. The terms activation and oxidation are used equivocally in this work.

The activation process causes a film with open pores to grow on the surface of the GC. The film growth law for thermochemical activation exhibits a complex sigmoidal characteristics [9,10]. For electrochemical activation, the film growth seems to have a simple linear growth characteristics [3,10]. The opened pores are accessible to gases or liquids and provide a huge specific internal surface area, which can be utilized as an electrode material for electrochemical double layer capacitors [1,4,5,7,8,14].

Differential electrochemical mass spectrometry performed on the G-type GC had revealed that CO_2 is the main reaction product during activation at 2.2 V versus Pd/H_2, and to a lesser extent, H_2. The evolution of CO_2 means then, that carbon is burned off. Evolution of oxygen could be ruled out. Reduction at 0.0 V versus Pd/H_2 causes evolution of CO_2, most likely due to the reduction of the surface groups created during oxidation. Upon further reduction, H_2 evolution occurs. X-ray photoelectron spectroscopy with respect to the carbon K-shell showed that activation creates carbonyl and/or quinone, and carboxyl surface groups, a well observed and studied phenomena on oxidized carbon

* Corresponding author. Present address: Consortium for Fossil Fuel Science, University of Kentucky, Suite 107 Sam Whalen Bldg., 533 South Limestone Street, Lexington, KY 40506, USA. Tel.: +1-859-257-6087; fax: +1-859-257-7215.
E-mail address: artur.braun@alumni.ethz.ch (A. Braun).
[1] ISE member.

0013-4686/$ – see front matter © 2003 Elsevier Ltd. All rights reserved.
doi:10.1016/j.electacta.2003.10.022

materials [2]. The reduction of the surface functional groups on the high-temperature forms of GC, which have less internal surface area than the low-temperature forms of GC [18], turned out to be more effective than for the low-temperature form.

During our studies on GC, it turned out that not only the kind of activation process, but also that the thickness of the GC as well as its heat treatment temperature (HTT) represent important activation parameters [19]. Depending on the HTT, GC is referred to as K-type GC (HTT around 1000 °C) or G-type GC (HTT around 2000 °C). It has turned out that the K-type is favorable for thermochemical activation, while G-type is more favorable for electrochemical activation [2,3]. Both materials and processes have their pros and cons with respect to supercapacitor applications. The present type of material received the same pyrolysis temperature like the G-type GC, but showed, maybe due to its thinness, a more graphite-like structure and significantly deviates from the aforementioned materials in terms of electrochemical performance for supercapacitor applications.

Unlike thermochemical activated GC, electrochemically activated GC requires a subsequent electrochemical reduction in order to get a significantly high double layer capacity (in this context, we refer to as *reduced* GC when we mean activated and subsequently reduced GC). However, electrochemical oxidation of G-type GC yields electrodes with a better frequency characteristics of the electrochemical double layer capacity [2], which amounts in a higher *power density* for the supercapacitor [14]. The monolithic, bipolar supercapacitor cell assembly [1,4,5] requires a well tuned ratio between active film thickness and non-activated GC core to obtain a high *energy density*. Because of diffusive and kinetic limitations in active film growth [3,9,10] and film brittleness on thick samples, thin GC plates are required for supercapacitor stacks.

To further explore the limits of electrochemical activation, we chose to study a relatively thin G-type form of pyrolytic carbon. This material showed striking differences from the previously studied GC, because it had a greyish surface texture and could be cut easily with a knife. Electrochemical observations on the present material made during oxidation and reduction are very similar to those known from graphite in sulfuric acid, i.e. the generation of electrochemical graphite oxide and changes of the surface color. Structural analysis, such as X-ray diffraction and small-angle neutron scattering, reveal that the present material cannot be considered GC anymore, but rather represents an intermediate state between GC and graphite.

2. Experimental

Pyrolytic carbon sheets (48 μm thickness, HTT 2200 °C) were purchased from Hochtemperaturwerkstoffe HTW GmbH, Thierhaupten/Germany. These had a grey color with a reflecting metal-like texture. Also, they could be cut easily with a knife in rectangular pieces, while conventional GC samples resist such attempts and break into many parts of irregular shape. See Fig. 1 for details about electrode preparation.

From the sheets, long stripes were cut with a length of 3.5 cm and a width of 1.2 cm, as shown in Fig. 1a. The boundaries of the stripes were covered with lacomite varnish to confine the conductivity to this part of the electrode, and to minimize inhomogeneities in the current distribution during electrochemical experiments. Using the varnish, a

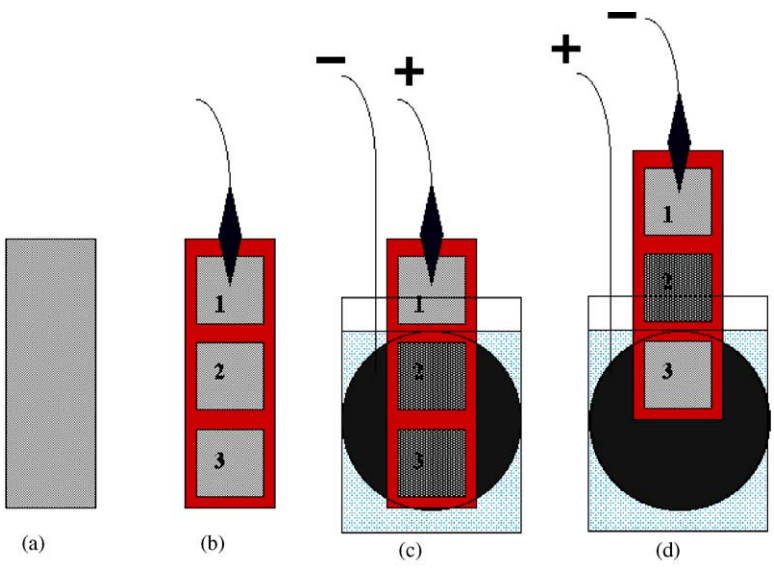

Fig. 1. Schematic of electrode preparation. Rectangular piece was cut from sample (a), coated with lacomite varnish to obtain sample parts 1–3 (b), and placed in an electrochemical cell with sample counter electrodes, sulfuric acid and reference electrode (not shown) (c) so that samples 2 and 3 were activated. Partial lifting of the GC stripe guaranteed that only sample 3 was reduced (d).

pattern was drawn on both sides that created three rectangular windows of 1 cm × 1 cm in size, as displayed in Fig. 1b. Once in the electrolyte, only the sample part marked by the windows would be exposed to the electrolyte. This technique allows for a better control of activation and quantification of the double layer capacitance. With 1 cm^2 window area, we typically could limit the error in double layer capacitance per sample area due to penetration of electrolyte between varnish and porous GC film to better than 5%. Two glassy carbon disks with 1 mm thickness and 5 cm diameter (K-type, pyrolyzed at 1000 °C) were used as a pair of counter electrodes, and the working electrodes were placed between these electrodes, with a distance of approximately 1 cm to either counter electrode. This set-up was efficient and provided samples with the same properties like samples obtained from a set-up with separate, single samples.

Experiments were carried out in 3 M H_2SO_4 using a potentiostat/galvanostat (EG&G 273A) and an impedance/gain-phase analyzer (Solartron SI 1260). The reference was a saturated calomel electrode (SCE). Electrochemical impedance spectra (EIS) were recorded at a potential of 0.9 V versus SCE over a frequency range from 0.1 to 100 kHz.

From the imaginary part of the impedance, Im(Z), the specific double layer capacitance C_A(f) (F/cm^2) of the sample with the exposed area A was determined for the frequency $f = 0.1$ Hz using the following relation:

$$C_A(f) = \frac{-1}{2\pi f \cdot \mathrm{Im}(Z) \cdot A}. \quad (1)$$

Activation potential was 2.07 V versus SCE, and the reduction potential was −0.5 V versus SCE. Fig. 1c shows the situation where two samples are activated at the same time under almost identical conditions.

After activation, a cyclic voltammogram (CV) of the activated sample was recorded with a scan rate of $\nu = 10$ mV/s over a potential range from 0.00 to 1.00 V, and this CV was attributed to both the sample at the bottom and at the middle. The CV was corrected for the effect of the double area.

Thereafter, the sample was lifted so that only the bottom sample was still in the electrolyte, but not the one in the middle, as displayed in Fig. 1d. Then, a CV was recorded which was assigned to the sample at the bottom. After that, the bottom sample was reduced, and then another CV was recorded, which was assigned to the bottom sample only. This procedure allows to provide two samples activated under almost identical conditions, one of which is oxidized and one of which is reduced. After the electrochemical experiments were completed, samples 1–3 were cut into separate parts. Sample 1 served as non-activated reference; samples 2 and 3 were rinsed with de-ionized water and dried under ambient atmosphere.

Small-angle neutron scattering was carried out ex-situ at the Swiss Spallation Neutron Source (SINQ) in Villigen, with neutrons of a wavelength of 8 Å. The samples were placed between two aluminium disks, which served as the sample holder, and a cadmium disk was on top of this assembly, facing to the detector in order to absorb parasitic scattering contribution. The intensity data were corrected for background noise, sample transmission and illuminated sample volume. Variation in the efficiency of different detector elements of the two-dimensional detector was corrected by referring to the incoherent scattering of a reference H_2O water sample.

The two-dimensional SANS data of all samples were found to be isotropic and were therefore averaged with respect to the azimuthal angle. Internal surface area data here are reported and compared in arbitrary units, since SANS intensity data were not available in absolute scattering length units. Comparison of relative SANS intensities yields accurate results. Also, data derived from Q-dependent considerations, such as Guinier analysis, are accurate. We have chosen small-angle scattering before gas adsorption techniques for surface area determination, because the latter technique showed unreasonably low surface areas for samples that had been exposed to the electrolyte (≈3.5 m^2/g). Additionally, the former technique was successfully applied to thermochemical activated samples and gave results comparable with N_2 adsorption [6].

3. Results

3.1. Capacitance

Fig. 2 displays cyclic voltammograms (CVs) of samples 1–3, as described in the previous section. All data concern the same original sample, but at different stages of treatment. While scanning the CV at 10 mV/s, the non-activated sample shows current densities of up to ±4 μA/cm^2. The activated sample shows a current density of around ±2 mA/cm^2, and the reduced sample shows current densities about as half as large as of the activated sample: ±1 mA/cm^2. The charge under the voltammogram increases considerably with activation time and is a direct measure for the increased double

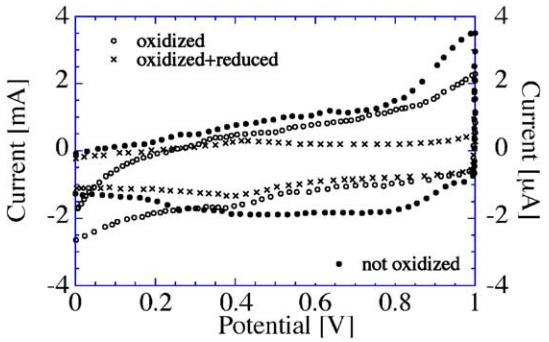

Fig. 2. Cyclic voltammograms of sample 1 (not oxidized, ●), sample 2 (oxidized, ○), and sample 3 (oxidized and reduced, ×). The axis on the right refers to sample 1.

layer capacity [3]. Current maxima evolving around 0.4 V versus SCE can be attributed to active surface groups of the quinone type [18,20].

The non-activated sample shows a significantly lower current density than the two activated samples. In fact, the currents differ by three orders of magnitude. Electrochemical activation of glassy carbon creates a large and electrochemically accessible internal surface area, which creates higher double layer capacity to be charged and discharged during cycling, such as like in the 1 mm thick G-type GC [2,3]. For the present material of 48 μm thickness, we make the same observation. It is remarkable however that the reduced sample has a lower current density than the activated sample. Note, that typical G-type GC with 1 mm thickness shows the opposite effect: a larger current density after reduction.

The capacitance measured with EIS at 0.1 Hz was 36.5 mF/cm^2 after 5 min of oxidation and 22.2 mF/cm^2 after subsequent reduction. The ratio of capacitance is 1.64. The capacitance at 0.1 Hz was around 440 mF/cm^2 for the 1 h oxidized, and 236 mF/cm^2 for the subsequently reduced sample. The ratio of the capacitance is 1.86. It is recalled that non-activated GC has a capacitance of only 20 μF/cm^2 [6,18]. Using this value, the electrochemically active surface area can be calculated.

We have observed that the sample changed its surface color from a shiny grey metal glance towards a matt black after oxidation. Upon reduction, the shiny grey surface color re-appeared. Similar observations have been made in the past by Beck et al. [21].

3.2. SANS

The dried samples were measured with SANS to obtain information on the internal surface area. After Porod, the internal surface area S of an irradiated sample volume V in a two-phase system with sharp boundaries, such as the carbon matrix with pores, can be obtained from the scattered intensity $I(Q)$ due to following relation [22–26]:

$$\lim_{Q\to\infty} I(Q) \propto 2\pi\Delta\eta^2 \frac{S}{V} \quad (2)$$

with $\Delta\eta^2$ being the scattering contrast between carbon matrix and pores. It has been shown in the past that Porod's law, i.e. the assumption of a clear phase separation between carbon matrix and pores, is valid for a whole range of carbon materials, including glassy carbon [27]. Since the present SANS data have been normalized to the irradiated sample volume V, we are able to compare the relative specific surface areas S/V of different samples, without specific knowledge of the scattering contrast $\Delta\eta^2$.

The scattering curves of the 1 h activated samples and the non-activated sample are displayed in Fig. 3 in a Porod plot. In a Porod plot, the intersection of the extrapolation of the scattering curves for large Q values with the abscissa yields the Porod constant, which is proportional to the internal surface area of the samples [22–26].

By comparison of the three scattering curves, it becomes evident that, upon activation, the internal surface area of the whole sample increases by a factor of around 2.8 from 2.3 to 6.5 a.u. However, after reduction the internal surface area decreases from 6.5 to 4.4 a.u.

The active film growth in glassy carbon plates during activation takes place beginning at the outer surface, and the active film propagates into the sample interior, surrounding an unreacted core with closed pores.

While we have succeeded in previous experiments to determine the active film thickness quite accurately, when electrochemical activation was carried out on thicker G-type samples [3], it was not possible to make a meaningful film thickness determination for the present material due to its rougher surface texture.

However, by knowledge of the capacitance data for activated GC, we can make a reasonable approximation for the film thickness in the present samples: The volumetric capacitance of activated K-type and G-type GC is about 100 F/cm^3

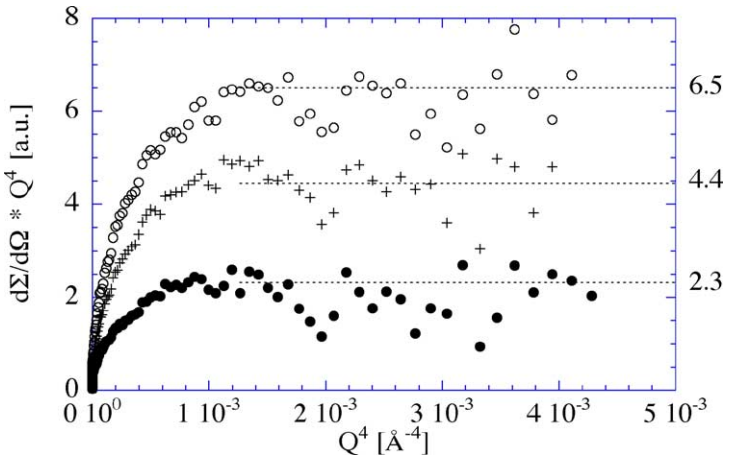

Fig. 3. SANS Porod plots of sample 1 (not oxidized, ●), sample 2 (oxidized, ○), and sample 3 (oxidized and reduced, ×).

[3,6]. The capacitance per geometric area is 440 mF/cm^2 for the 1 h activated sample. To obtain this value, a film thickness of 44 μm is required. Since the sample thickness here is about 48 μm, we can conclude that almost the entire sample is activated. This finding is in line with the drastic sample expansion upon activation, which we will discuss in the following section. We thus can form the direct ratio of the Porod constants for the activated and the reduced sample

$$\frac{P_{ox}}{P_{red}} = \frac{6.5}{4.4} \approx 1.48\,; \tag{3}$$

this is a lower limit for the ratio of the Porod constants.

An upper limit is obtained when we subtract the scattering contribution of the non-activated GC

$$\frac{6.5 - 2.3}{4.4 - 2.3} = 1.97 > \frac{P_{ox}}{P_{red}}\ . \tag{4}$$

The ratio of SANS internal surface areas prior to, and after reduction (1.48–1.97) matches the ratio of the electrochemical double layer capacitance prior to and after reduction surprisingly well (1.86). The good match reveals that the surface areas of the electrochemically treated samples as measured with SANS are indeed accessible for electrolytes and represent electrochemically active surface area.

Fig. 4 shows the scattering curves in log–log representation. The original SANS curves have a power law decay of the intensity in the range 0.003 Å^{-1} ≤ Q ≤ 0.56 Å^{-1}, with an exponent of -3 ± 0.1. For higher Q, they show a tail with a lower order of decay, which is typically caused by a convolution of constant background scattering and scattering from characteristic structures. To further resolve these structures, the power law of Q^{-3} and constant background scattering were subtracted from the original SANS curves.

The solid lines (—) in Fig. 4 represent least square fits of a Guinier function

$$I(Q) \propto I_0 \exp\left(\frac{-Q^2 R_g^2}{3}\right) \tag{5}$$

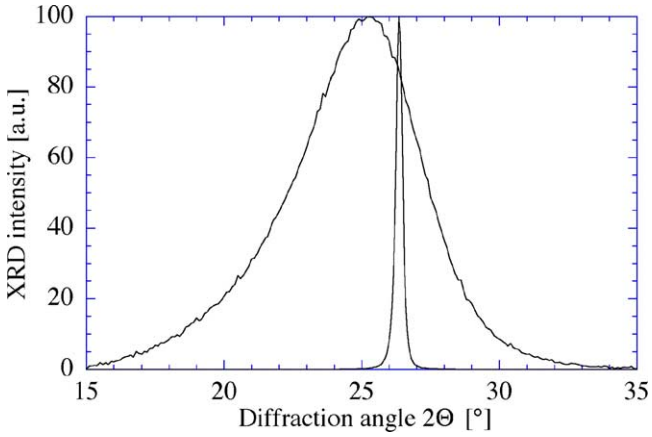

Fig. 5. X-ray diffractograms of G-type glassy carbon with HTT 2200 °C (broad reflex) and pyrolytic carbon with same HTT, but 48 μm thickness (sharp reflex).

to structures at high Q, which originate from the scattering of micropores or mesopores [28]. According to the IUPAC nomenclature [29], micropores are pores with widths not exceeding 2 nm, and mesopores are pores with widths between 2 and 50 nm. The radii of gyration R_g quantifies the electron density distribution, in analogy to the radius of inertia for mass density distribution in mechanics. For spheres, R_g and the geometrical radius R are linked via the relation

$$R = R_g \cdot \sqrt{\frac{5}{3}}. \tag{6}$$

The radii of gyration R_g for either micropore scattering contributions were 12.0 Å for the non-activated GC, and 12.7 (11.5) Å for the 1 h activated (and reduced) sample, respectively. This translates into sphere diameters of 30.9, 32.7, and 29.5 Å, respectively.

Fig. 5 shows X-ray diffractograms of two phenolic resins pyrolyzed at 2200 °C. Both materials received the same treatment by the manufacturer, but their initial precursor thicknesses were different. The thicknesses after high

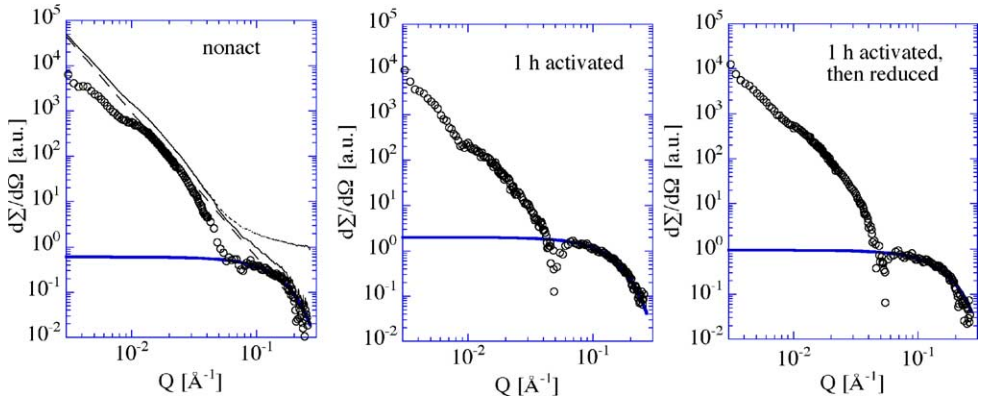

Fig. 4. log–log plots of non-activated and 1 h activated/reduced samples, after subtraction of a power law with Q^{-3} and constant background (open symbols). Left plot shows the original SANS curve (···), SANS curve after constant background subtraction (—), as well as the power law fit (- - -). Solid lines (—) in all three plots are least square fits to Guinier function.

temperature pyrolysis were 48 μm and 1 mm, respectively. The diffractogram of the 1 mm thick GC shows a relatively broad (0 0 2) Bragg reflex, which is typical for GC. In contrast, the thin 48 μm sample has a very sharp (0 0 2) Bragg reflex. Both reflexes can be indexed as the (0 0 2) Bragg reflex of graphite with PDF 14-1079 [30]. The peak position of the thin sample is at 26.38°, which yields 3.47 Å for the graphene sheet distance, after Bragg's diffraction law. The peak position of the 1 mm thick glassy carbon is found at a lower diffraction angle, 25.29°, indicating that the graphene sheets are wider apart (3.61 Å), at average. Note that the graphene layer distance in graphite is 3.35 Å.

The very narrow full width at half maximum (FWHM) of the (0 0 2) Bragg reflex is another property which this kind of pyrolyzed phenolic resin shares with graphite. From the FWHM, we were able to estimate the crystallite size by using the Scherrer formula [6,30]. Based on the Scherrer formula,

$$L_c = \frac{\alpha \cdot \lambda}{B \cos\theta} \quad (7)$$

we estimated the crystallite sizes L_c of both materials [30]. Here, λ is the X-ray wavelength of Cu Kα radiation, 1.54056 Å, B the full-width at half-maximum, and θ the position of the (0 0 2) Bragg reflex. The shape factor α accounts for perturbations in the coherence of the crystallites and may vary from 0.9 to 1.89, depending on the material. For carbonaceous materials, α is typically found to be around 0.9 [31]. L_c was found to be about 15 Å for the GC and about 300 Å for the pyrolytic carbon. In this case, strain in the samples and instrument broadening can be neglected. Note, that transmission electron microscopy may often yield crystallite sizes larger than measured with XRD [30]. Both diffractograms show striking differences in peak widths, and consequently, the material studied in the present paper cannot be considered a typical glassy carbon.

The internal surface area as measured with small-angle scattering concerns the geometrical internal surface area, regardless whether it is accessible to fluids, or not. Since the capacitance decreases to the same extent as the internal surface area, it may be concluded that the pores are not simply closed by some effect. More likely, a collapse of the pore network upon the reduction may be one explanation for the decrease of the internal surface area and capacitance.

3.3. Thickness changes

We found that after electrochemical treatment (oxidation and reduction), the samples had experienced remarkable thickness changes. Thicknesses were measured with a *Stylus* profile detector; data are summarized in Table 1. Prior to the thickness determination, all samples were dried in vacuum oven at 70 °C. The sample thickness depended on whether the detector tip on the sample was pressurized or not. Thicknesses were determined for *no pressure* (this is when only the detector tip with negligible weight rested on the sample) and for ca. 0.5 N/mm^2.

After oxidation, the sample thickness increased by around 40% (100%, when no significant pressure was applied). After reduction, the thickness decreased again to a value which was still higher than the original thickness.

It is noteworthy that this particular kind of "glassy carbon" samples can be easily pressed with a tip by hand so that the sample thickness decreases from somewhat over 50\μ∼ m to 46\μ∼ m. While glassy carbon is generally considered a hard carbon [15], we believe that the particular material here is neither purely glassy carbon nor graphite, but an intermediate phase which carries properties of both. K-type GC of the same thickness and G-type GC with higher thicknesses do not show such flexibility and permit not such thickness changes upon pressurizing.

4. Discussion

Since the fundamental work of Rüdorff and Hoffmann [32], it is well known that graphite can be electrochemically oxidized to form a macrocation, while certain anions are being inserted between the graphite lattice planes (intercalation), such as HSO_4^-. Intercalation of anions causes an expansion of the graphite lattice distance. Intercalation of anions into graphitic materials and their corrosion in aqueous electrolytes has been subject to numerous studies in the past, cf. [21,33–37].

We attribute the swelling of the samples after activation and the shrinking after subsequent reduction to major structural changes between GC matrix and the enclosed pores, or even to a degradation of the GC matrix. This seems to be the macroscopic manifestation of changes in the interlayer spacing of a carbonaceous material with graphitic order, when intercalation of anions occurs, and the generation of graphite oxide and its subsequent dissolution upon subsequent reduction. Such changes have been observed and quantified in graphite for many years using dilatation or diffraction methods. Our laboratory has recently published results on the expansion of the interlayer spacing on a local microscopic scale [37]. This experiment concerned highly

Table 1
Sample thickness and mass per sample area for non-activated and electrochemically treated thin SIGRADUR® G sheets with 48 μm thickness (1 h activated, 15 min reduced)

Pressure	Thickness (μm)			Mass density (mg cm^{-2})		
	Non-activated	Activated	Activated + reduced	Non-activated	Activated	Activated + reduced
No pressure	55–56	106 ± 13	77.5 ± 12			
0.5 N/mm^2	47–48	67 ± 1	55 ± 4	13.6 ± 0.5	14 ± 0.2	10.9 ± 0.3

oriented pyrolytic graphite (HOPG). In there, changes in the interlayer spacing ranged from 14 to 32%, depending on whether thousands or tens of graphene layers were involved by the intercalation, respectively.

The material under investigation here has a much lower degree of crystallinity than HOPG, but a higher degree of crystallinity than glassy carbon. This is obvious from the XRD diffractograms. It is known as a rule of thumb [38] that high crystallinity in carbon is a strong requirement for a reversible intercalation of suitable anions. Such highly crystalline graphitic materials have a very low internal surface area. Carbonaceous materials of very low crystallinity do not permit intercalation, but they are very prone to surface oxidation, which results in the presence of oxygen containing surface groups [39,40]. Overoxidation of graphite is limited because the electronic conductivity significantly decreases during oxidation, and it can be reduced to graphite with 100% current efficiency. Reduction, however, leads to a structural distortion of the graphite [41].

We have carried out X-ray photoelectron spectroscopy analysis of electrochemically oxidized and reduced G-type and K-type glassy carbon. For the non-activated G-type, the oxygen content was 3%, but increased to 28.4% after oxidation (1.95 V versus SCE), and decreased to 11.22% after reduction (-0.3 V versus SCE). For the K-type, the oxygen content was 6.5%, but increased to 30.2% after oxidation, and decreased to 22.6% after reduction. The G-type GC has wider pores and less surface area than the K-type, and this is the most likely explanation why we find less oxygen in G-type GC [15,42]. Interestingly, thermochemical activation of the K-type at temperatures from 400 to 500 °C yields oxygen concentrations ranging from 6.5 to 11.8%, respectively.

The SANS results clearly show that the samples contain pores, same like glassy carbon, and thus a considerable internal surface area. This holds also for the non-oxidized sample. The cyclic voltammograms of the non-oxidized and oxidized sample clearly indicate that the internal surface becomes accessible for the electrolyte during oxidation. The oxidation causes a pore enlargement from $R_g = 12.0$ to 12.7 Å. Such a pore growth is known to cause a decrease of the overall internal surface area [6,7], because pores coalesce and thus pore walls which contribute to the surface area, are being removed. Subsequent reduction, however, should not necessarily create new pore walls.

However, during reduction R_g decreases from 12.7 to 11.5 Å. A possible explanation for this could be, that reduction removes surface functional groups which were created by the previous oxidation, and graphene sheets fall close together and build smaller pores, similar as the so-called *falling cards model* as proposed by Xue and co-workers[43]. Since the decreased capacitance after reduction was found in-situ while samples were still in electrolyte, the decrease of the internal surface area cannot be explained by the drying of the samples. The decreasing capacitance and internal surface area, the volume and mass changes support the suggestion that a collapse of the pore network occurs during reduction.

SIGRADUR® G sheets with 48 μm nominal thickness and the corresponding disks with 1 mm thickness deviate considerably from each other with respect to their behavior after electrochemical oxidation and reduction. We have observed that the GC changed its surface color from a shiny grey metal glance towards a matt black after oxidation. Upon reduction, the shiny grey surface color re-appeared.

Possibly, structural differences explain why the 1 mm samples keep their consistency during electrochemical activation and reduction, while the thin sheets experience a drastic degradation.

For two-phase systems with sharp transition of the electron density at the interface, the exponent of decay is −4 [22–24]. Exponents lower than −4 are then interpreted as arising from systems with less sharp electron transitions. For non-graphitizable carbons, such as glassy carbon, the exponent of decay is reportedly a function of the heat treatment temperature of the material [28,44], and the exponent of decay is closer to −4, the higher the HTT was. This holds in particular for GC which has experienced a HTT of more than 2000 °C. The carbon material in the present study has received a HTT of 2200 °C, but the exponent of decay is −3, in contradiction to traditional findings for GC.

Their structural differences were also obvious from their XRD diffractograms. The thin sheets have larger and sharper Bragg reflexes and therefore larger crystallites than the 1 mm thick samples. On the other hand, the 48 μm thick samples show a pronounced Guinier range for micropores and subsequent intensity plateau, which is typical for glassy carbon.

5. Conclusion

We have shown that a very graphitic form of pyrolytic carbon can be electrochemically oxidized and thus activated, similar like glassy carbon, provided an inherent porosity is present. Unlike glassy carbon, however, pyrolytic carbon with a high degree of graphitization does not provide a higher double layer capacitance after subsequent electrochemical reduction. In contrast, the electrochemical double layer capacity as well as the entire internal surface area of the pyrolytic carbon exhibit a significant decrease upon reduction. With respect to potential applications as supercapacitor electrodes, there seems to be a limit to which pyrolytic carbon can be used for such electrodes. The G-type GC with 2200 °C heat treatment temperature was shown to have excellent figures of merit as a supercapacitor electrode material [2,3]. The pyrolytic carbon studied in the present work must be ruled out for such applications due to poor structural integrity after electrochemical treatment, as well as due to a lower electrochemical double layer capacity than comparable carbon materials. G-type GC and the material studied here significantly differ in their structure, as observed with XRD and simple mechanical tests. It is likely that the

structural properties of carbon thus hold also valuable key information for its electrochemical performance and future structural integrity. It is therefore advisable to carry out typical structure analyses, such as like X-ray diffraction, for the quest of optimized materials for supercapacitor electrodes.

Acknowledgements

Financial support by the Board of the Swiss Federal Institute of Technology (Swiss Priority Program on Materials Research) is gratefully acknowledged. Part of this work was performed at the Swiss Spallation Neutron Source, Paul Scherrer Institut, Villigen, Switzerland.

References

[1] J. Miklos, K. Mund, W. Naschwitz, Siemens AG, Offenlegungsschrift DE 30 11 701 A1, Deutsches Patentamt, 1980.
[2] M.G. Sullivan, R. Kötz, O. Haas, J. Electrochem. Soc. 147 (1) (2000) 308.
[3] M.G. Sullivan, B. Schnyder, M. Bärtsch, D. Alliata, C. Barbero, R. Imhof, R. Kötz, J. Electrochem. Soc. 147 (7) (2000) 2636.
[4] M. Bärtsch, A. Braun, R. Kötz, O. Haas, in: Proceedings of the 38th Power Sources Conference, Cherry Hill, NJ, 1998.
[5] M. Bärtsch, A. Braun, B. Schnyder, R. Kötz, O. Haas, J. New Mater. Electrochem. Syst. 2 (1999) 273.
[6] A. Braun, M. Bärtsch, B. Schnyder, R. Kötz, O. Haas, H.-G. Haubold, G. Goerigk, J. Non-Cryst. Solids 260 (1/2) (1999) 1.
[7] A. Braun, M. Bärtsch, F. Geiger, B. Schnyder, R. Kötz, O. Haas, M. Carlen, T. Christen, C. Ohler, P. Unternährer, E. Krause, in: Proceedings of the Materials Research Society 575 (1999) 369.
[8] A. Braun, Dissertation ETH Zürich no. 13292, 1999.
[9] A. Braun, M. Bärtsch, B. Schnyder, R. Kötz, Chem. Eng. Sci. 55 (22) (2000) 5245.
[10] A. Braun, A. Wokaun, H.-G. Hermanns, Appl. Math. Modell. 27 (2003) 47.
[11] W. Gille, A. Braun, J. Non-Cryst. Solids 321 (2003) 89.
[12] A. Braun, M. Bärtsch, O. Merlo, B. Schnyder, B. Schaffner, R. Kötz, O. Haas, A. Wokaun, Carbon 41 (4) (2003) 759.
[13] A. Braun, M. Bärtsch, B. Schnyder, R. Kötz, O. Haas, A. Wokaun, Carbon 40 (3) (2002) 375.
[14] R. Kötz, M. Carlen, Electrochim. Acta 45 (2000) 2483.
[15] G.M. Jenkins, K. Kawamura, Polymeric carbons—carbon fibre, glass and char, first ed., Cambridge University Press, Cambridge, UK, 1976.
[16] J.C. Lewis, B. Redfern, F.C. Cowlard, Solid State Electron. 6 (1963) 251.
[17] F.C. Cowlard, J.C. Lewis, J. Mater Sci. 2 (1967) 507.
[18] K. Kinoshita, Carbon—Electrochemical and Physicochemical Properties, Wiley, New York, 1988.
[19] A. Braun, Effect of sample thickness and pyrolysis temperature on the activation of glassy carbon, in preparation.
[20] C. Barbero, J.J. Silber, L. Sereno, J. Electroanal. Chem. 248 (1988) 321.
[21] F. Beck, H. Krohn, E. Zimmer, Electrochim. Acta 31 (3) (1986) 371.
[22] G. Porod, Kolloid Z. Z. Polym. 124 (2) (1951) 83.
[23] G. Porod, Kolloid Z. Z. Polym. 125 (1) (1952) 51.
[24] G. Porod, Kolloid Z. Z. Polym. 125 (2) (1952) 109.
[25] O. Glatter, O. Kratky, Small-Angle X-Ray Scattering, Academic Press, New York, 1982.
[26] L.A. Feigin, D.I. Svergun, Structure Analysis by Small-Angle X-Ray and Neutron Scattering, Plenum Press, New York, 1987.
[27] W. Ruland, Carbon 39 (2001) 323.
[28] R. Perret, W. Ruland, J. Appl. Cryst. 5 (1972) 183.
[29] IUPAC, Pure Appl. Chem. 57 [4] (1985) 603–619: Reporting physisorption data for gas/solid systems: pores with widths exceeding about 50 nm are called macropores, pores of widths between 2 and 50 nm are called mesopores, and pores with widths not exceeding about 2 nm are called micropores.
[30] V.A. Drits, T. Tchoubar, X-ray Diffraction by Disordered Lamellar Structures, Springer–Verlag, Berlin, 1990.
[31] B.E. Warren, G.S. Gingrich, Phys. Rev. 46 (1934) 368.
[32] W. Rüdorff, U. Hoffmann, Z. Anorg. Allg. Chem. 238 (1938).
[33] F. Beck, H. Junge, H. Krohn, Electrochim. Acta 26 (7) (1981) 799.
[34] E. Frackowiak, W. Kaiser, H. Krohn, F. Beck, Mol. Cryst. Liq. Cryst. Sci. Technol. A 244 (1994) 221.
[35] J. Fiang, F. Beck, Carbon 30 (2) (1992) 223.
[36] U. Tormin, F. Beck, Electrochim. Acta 40 (12) (1995) 1955.
[37] D. Alliata, R. Kötz, O. Haas, Langmuir 15 (1999) 8483.
[38] H. Thiele, Z. Elektrochem. 40 (1934) 26.
[39] H.-P. Boehm, E. Diehl, W. Heck, R. Sappok, Angew. Chem. 76 (1964) 742.
[40] H.-P. Boehm, M. Voll, Carbon 8 (1970) 227.
[41] J.O. Besenhard, Z. Naturforsch. B32 (1977) 1210.
[42] A. Braun, M. Bärtsch, B. Schnyder, R. Kötz, O. Haas, PSI Scientific Report 1998 V (1999) 34, ISSN 1423-7342.
[43] W. Xing, J.S. Xue, T. Zheng, A. Gibaud, J.R. Dahn, J. Electrochem. Soc. 143 (11) (1996) 3482.
[44] R. Perret, W. Ruland, J. Appl. Cryst. 1 (1968) 308.